Journal of the European Ceramic Society **19** (1999) 1191–1195

PII: S0955-2219(98)00402-6
0955-2219/99/$ - see front matter

Piezoelectric and Structural Properties of $Pb(Yb_{1/2}Nb_{1/2})O_3$–$PbTiO_3$–$PbZrO_3$ Ceramics

Hiromu Ohuchi,* Sintarou Tsukamoto, Mitsuru Ishii and Hiromitsu Hayakawa

Department of Material Science and Ceramic Technology, Shonan Institute of Technology, Tsujido-nishikaigan Fujisawa Kanagawa, 251-8511 Japan

Abstract

Solid solution ceramics of the system $xPb(Yb_{1/2}Nb_{1/2})O_3$–$yPbTiO_3$–$zPbZrO_3$, *where* $x = 0{\cdot}1$–$0{\cdot}8$, $y = 0{\cdot}1$–$0{\cdot}7$, $z = 0{\cdot}1$–$0{\cdot}8$, *and* $x + y + z = 1$, *were prepared by the solid state reaction of powder materials. Ceramic, dielectric and piezoelectric properties and crystal structures of the system were studied. The system is composed of three crystal phases at room temperature: the monoclinic, tetragonal and rhombohedral. Sintering of the system* $xPb(Yb_{1/2}Nb_{1/2})O_3$–$yPbTiO_3$–$zPbZrO_3$ *is much easier than that of each end compositions and well sintered ceramics were obtained for the compositions near the structural transformation boundary. Piezoelectric ceramics with high electric permittivities, high radial coupling coefficient,* k_r, *and low mechanical quality factor were obtained for the compositions near the structural transformation. The composition* $Pb(Yb_{1/2}Nb_{1/2})_{0{\cdot}1}Ti_{0{\cdot}48}Zr_{0{\cdot}42}O_3$ *showed the highest* k_r of 0·61. © *1999 Elsevier Science Limited. All rights reserved*

Keywords: $Pb(Yb_{1/2}Nb_{1/2})O_3$–$PbTiO_3$–$PbZrO_3$ ceramics, dielectric properties, piezoelectric properties.

1 Introduction

It is known that piezoelectric ceramics are generally ferroelectric material with perovskite-type structure. To make piezoelectric ceramics, it is necessary that the crystal unit cells of the material have no center of symmetry. Furthermore, it should also be possible to orient the spontaneous polarization in the crystallographic directions by an externally applied field.

*To whom correspondence can be addressed. Fax: +81-466-36-1594; e-mail: oouchi@mate.shonan-it.ac.jp

Jaffe *et al.*[1,2] succeeded in obtaining lead zirconate titanate ceramics from the solid solution of $PbTiO_3$ (ferroelectric, tetragonal) and $PbZrO_3$ (antiferroelectric, orthorhombic). After discovery of piezoelectric properties in the binary system lead zirconate titanate, studies on piezoelectric ceramics were expanded to develop more solid solution ceramics composed of multicomponent system. Smolenskii and Agranovskaya[3] showed a possible method of preparing complex compounds with perovskite structure. Much attention has focused on the piezoelectric properties of ternary system consisting of complex compounds for example $Pb(Mg_{1/2}Nb_{2/3})TiZrO_3$[4] and $Pb(Mg_{1/3}Ta_{2/3})TiZrO_3$.[5]

Yamamoto and Ohashi[6] developed solid solution ceramics of the binary system $PbTiO_3$–$Pb(Yb_{1/2}Nb_{1/2})O_3$ (antiferroelectric, monoclinic). However, there is no information on the electric properties in the ternary system $Pb(Yb_{1/2}Nb_{1/2})O_3$–$PbTiO_3$–$PbZrO_3$.

The purpose of the present work is to describe the ceramic, dielectric and piezoelectric properties of $Pb(Yb_{1/2}Nb_{1/2})O_3$–$PbTiO_3$–$PbZrO_3$ system. Another purpose of this work is to show a structural transformation boundary in the ternary system, a phenomenon expected from the difference in the crystal structures of each end compound at room temperature.

2 Experimental

2.1 Sample preparation

The ceramic samples of the system $xPb(Yb_{1/2}Nb_{1/2})O_3$-$yPbTiO_3$–$zPbZrO_3$, where $x = 0{\cdot}1$–$0{\cdot}8$, $y = 0{\cdot}1$–$0{\cdot}7$, $z = 0{\cdot}1$–$0{\cdot}8$ and $x + y + z = 1$, were prepared from chemical reagent grade PbO (99·99%), Yb_2O_3 (99·9%), Nb_2O_5 (99·9%), TiO_2 (98·65%), and ZrO_2 (99·9%) by solid state reaction of powder materials. Weighed raw material (1 batch = 35 g) of a given composition was wet-milled in a plastic mill

with partially stabilized zirconia balls (about 5 mm in diameter; total weight 100 g) and water (50 ml) for 17 h, dried and pressed into tablets at 40 MPa. The tablets were calcined at 850°C (a uniform heating rate of 5°C min^{-1}) for 2 h in a covered alumina crucible, cooled wet-ground for 17 h in a plastic mill and then dried. The ground material was mixed with polyvinyl alcohol (5 wt%) in a mortar and was pressed into disks 10 mm in diameter by about 2 mm in thickness at a pressure of 100 MPa. Five stacked disks were fired at 1000–1150°C (heating rate of 5°C min^{-1}) in an electric furnace on a platinum sheet covered with a magnesia crucible to minimize evaporation of PbO. The fired disks were ground to a thickness of about 0·5 mm, and silver paste was fired on the disk surfaces at 700°C as electrodes. Poling treatment was carried out in silicone oil at 100°C by applying a DC field of 4 kv mm^{-1} for 1 h, and samples were field cooled to room temperature in 30 min.

2.2 Measurement

2.2.1 Density and water absorption
The density of fired samples was determined by Archimedes method in water.

2.2.2 Linear shrinkage
The linear shrinkage was obtained by comparing the diameter of the disk-shaped samples before and after heat treatment.

2.2.3 X-ray analyses
X-ray powder diffraction examinations were made with a recording diffractometer (Rigaku Denki, RAD-RC) using CuK_α radiation through a nickel filter at room temperature. Prom these diffraction patterns, structural transformation boundaries were determined.

2.2.4 Electrical resistance measurements
The resistance was measured with an HP4329A high-resistance meter. The electrical resistivity was calculated from the resistance. thickness and diameter of samples.

2.2.5 Dielectric measurements
Capacitance and dissipation factor, tan δ, were measured at room temperature with an HP4192A impedance analyzer using a frequency of 1 kHz. The electric permittivity was calculated from the capacitance, diameter and thickness of samples.

2.2.6 Piezoelectric measurements
Twenty-four hours after poling, the piezoelectric property was measured with an HP4192A impedance analyzer by a method similar to that of the Institute of Radio Engineers Standards.[7] The resonant frequency, f_r, antiresonant frequency, f_a and resonant resistance R of the radial fundamental mode were measured at room temperature. Mechanical quality factor, Q_M was calculated from f_r, f_a, R and capacity (at 1 kHz).

3 Results and Discussion

3.1 Sintered density

It was difficult to obtain a well sintered body from each end composition of the ternary system, because $PbTiO_3$ has a large anisotropic crystallographic transformation at the Curie temperature of 490°C. $PbZrO_3$ shows intense volatization of PbO, and $Pb(Yb_{1/2}Nb_{1/2})O_3$ exhibits low sinterability. For example, $Pb(Yb_{1/2}Nb_{1/2})O_3$ ceramics fired at 1000°C for 45 min show density of 8·45 g cm^{-3}, shrinkage of 8·7% and water absorption of 2·3%. The $Pb(Yb_{1/2}Nb_{1/2})O_3$–$PbTiO_3$–$PbZrO_3$ compositions sintering is free of these difficulties. Their water absorption is less than 0·95% and the near structural transformation boundary composition becomes nearly 0% at optimum firing temperature from 1000 to 1100°C which is lower than that of $PbTiO_3$–$PbZrO_3$ binary compositions of 1220°C. Therefore, sintering of the ternary compositions becomes easier.

Figure 1 shows the effect of compositional dependence on the sintered density for $Pb(Yb_{1/2}Nb_{1/2})O_3$–$PbTiO_3$–$PbZrO_3$ solid solution ceramics at 1050°C for 45 min. Shrinkage (s), sintered density (d) and water absorption (w) for $Pb(Yb_{1/2}Nb_{1/2})$

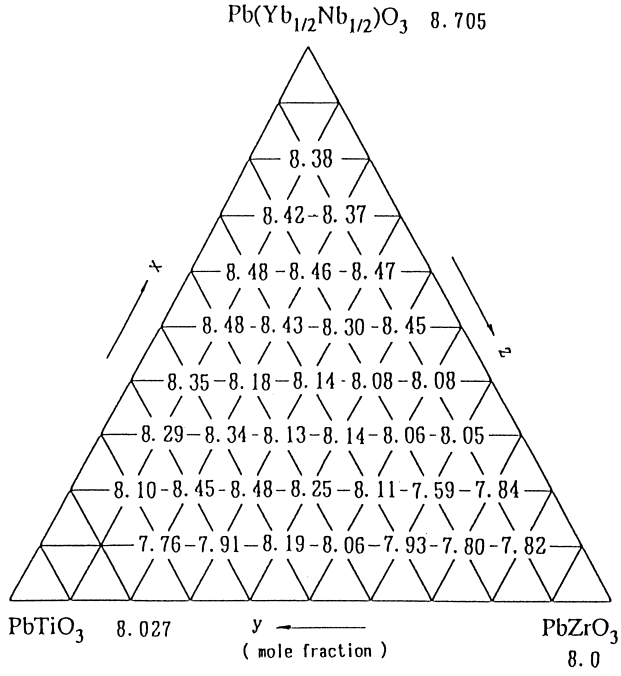

Fig. 1. Density for xPb($Yb_{1/2}Nb_{1/2}$)O_3–$y$$PbTiO_3$–$z$$PbZrO_3$ ($x+y+z=1$) ceramics sintered at 1050°C for 45 min (g cm^{-3}).

O_3–$PbTiO_3$–$PbZrO_3$ ceramics were obtained as $s = 13{\cdot}4$–$7{\cdot}7\%$, $d = 8{\cdot}48$–$7{\cdot}59\ g\,cm^{-3}$ and $w = 0{\cdot}00$–$0{\cdot}95\%$, respectively. Thus, well sintered and high density ceramics were obtained for compositions near the structural transformation boundary.

Grain structure of $Pb(Yb_{1/2}Nb_{1/2})_{0{\cdot}1}Ti_{0{\cdot}5}Zr_{0{\cdot}4}O_3$ ceramics with the near structural transformation boundary composition is fine and grain size of 2–3 μm was obtained. Grain growth for $Pb(Yb_{1/2}Nb_{1/2})_{0{\cdot}1}Ti_{0{\cdot}5}Zr_{0{\cdot}4}O_3$ ternary ceramics is inhibited as compared with the grain size of 13–7 μm for $PbTi_{0{\cdot}47}Zr_{0{\cdot}53}O_3$ binary ceramics.[8]

3.2 Phase relations

Figure 2(a) shows the relation between the composition studied in the ternary system $xPb(Yb_{1/2}Nb_{1/2})O_3$–$yPbTiO_3$–$zPbZrO_3$ and the crystal phase at room temperature. The solid solution of ternary system $Pb(Yb_{1/2}Nb_{1/2})O_3$–$PbTiO_3$–$PbZrO_3$ is composed of monoclinic, tetragonal and rhombohedral crystal phases. A structural transformation boundary between a tetragonal phase ($PbTiO_3$) and a monoclinic phase [$Pb(Yb_{1/2}Nb_{1/2})O_3$] occurred at $y = 0{\cdot}5$ to $0{\cdot}475$ mole fraction of $PbTiO_3$[6] and another structural transformation between a tetragonal and a rhombohedral phase ($PbZrO_3$) occurred at $y = 0{\cdot}45$ to $0{\cdot}475$ mole fraction of $PbTiO_3$.[2] In the ternary system, a structural transformation boundary from a tetragonal phase to a rhombohedral or a monoclinic phase is found in the vicinity of $y = 0{\cdot}48$–$0{\cdot}42$ mole fraction of $PbTiO_3$ for $x = 0{\cdot}1$, $0{\cdot}2$, $0{\cdot}3$ and $0{\cdot}4$ mole fraction of $Pb(Yb_{1/2}Nb_{1/2})O_3$. The tetragonal phase area is bounded by a convex curve to $PbTiO_3$.

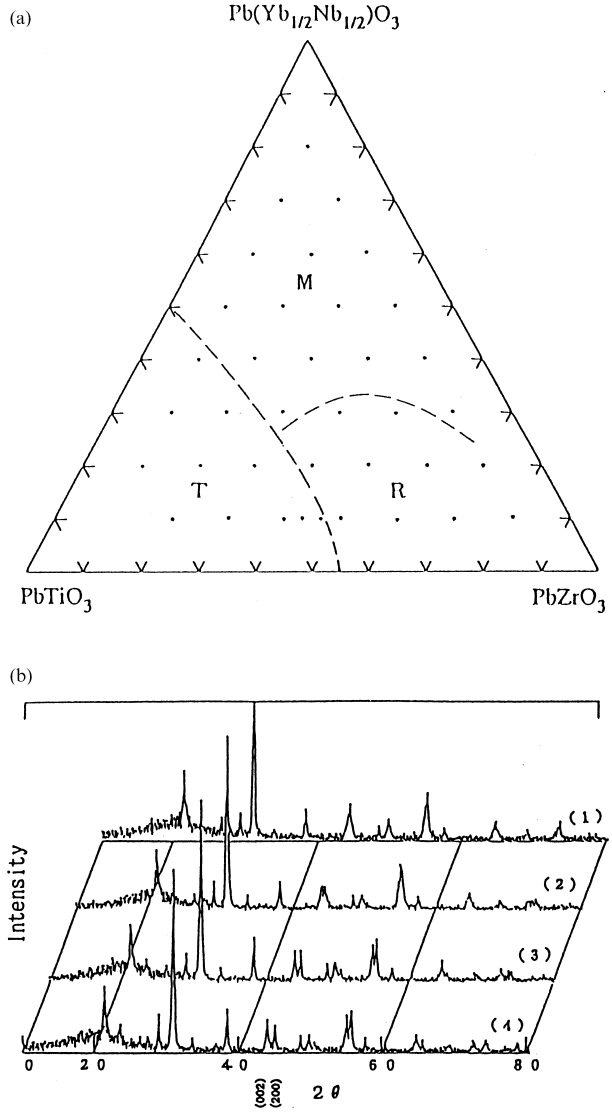

Fig. 2. (a) Phase diagram of ternary system $xPb(Yb_{1/2}Nb_{1/2})O_3$–$yPbTiO_3$–$zPbZrO_3$ ($x+y+z=1$). M = monoclinic, T = tetragonal, R = rhombohedral at room temperature. (b) X-ray diffraction pattern for $xPb(Yb_{1/2}Nb_{1/2})O_3$–$yPbTiO_3$–$zPbZrO_3$, where: (1) $x = 0{\cdot}1$, $y = 0{\cdot}4$; (2) $x = 0{\cdot}1$, $y = 0{\cdot}425$; (3) $x = 0{\cdot}1$, $y = 0{\cdot}45$; (4) $x = 0{\cdot}1$; $y = 0{\cdot}5$.

Figure 2(b) shows the relation of crystal phase versus 2θ at the near structural transformation boundary by X-ray analysis; in particular, when 2θ is within the range of 40–60°, a structural transformation is found from change of (002) and (200) peak. The (200) line profile of rhombohedral phase splits into (002) and (200) lines of tetragonal phase. A structural transformation boundary between the rhombohedral and the monoclinic phase is still uncertain but may be drawn a shown in Fig. 2(a) within the accuracy of the present experiment.

3.3 Electric properties

The electrical resistivity for the ternary system $xPb(Yb_{1/2}Nb_{1/2})O_3$–$yPbTiO_3$–$zPbZrO_3$ ceramics change with composition from $6{\cdot}25\times10^8$ to $0{\cdot}66\times10^8$ (Ω·m) and for most ceramics show electrical resistivity higher than 1×10^8 (Ω·m) and there was no break down during the poling treatment.

Figure 3 shows the relative electric permittivities ($\varepsilon_{33}^T/\varepsilon_0$) after poling for the ternary system $xPb(Yb_{1/2}Nb_{1/2})O_3$–$yPbTiO_3$–$zPbZrO_3$ with $xPb(Yb_{1/2}Nb_{1/2})O_3$ as a parameter. The relative electric permittivities and dissipation factor for the ternary system change with the addition of $Pb(Yb_{1/2}Nb_{1/2})O_3$ from 180 to 1470 and from 0·011 to 0·112, respectively. In each series of Fig. 3, the composition with maximum relative electric permittivities also coincides with the structural transformation between tetragonal and rhombohedral phases. This result is in agreement with the behavior described in the ternary system $Pb(Mg_{1/3}Nb_{2/3})O_3$–$PbTiO_3$–$PbZrO_3$.[4] The relative electric permittivities of $xPb(Yb_{1/2}Nb_{1/2})O_3$–$yPbTiO_3$–$zPbZrO_3$ at the structural transformation increases with increasing $Pb(Yb_{1/2}Nb_{1/2})O_3$ content up to $x = 0{\cdot}3$ and decreases with increasing $Pb(Yb_{1/2}Nb_{1/2})O_3$ content more than $x = 0{\cdot}4$.

Figure 4 shows the radial coupling coefficient for the ternary system $xPb(Yb_{1/2}Nb_{1/2})O_3$–$yPbTiO_3$–$zPbZrO_3$ with $xPb(Yb_{1/2}Nb_{1/2})O_3$ as a parameter.

The radial coupling coefficient change with composition from 0·16 to 0·61 for the composition $x \leqq 0{\cdot}6$. Piezoelectric properties of $x\mathrm{Pb}(\mathrm{Yb}_{1/2}\mathrm{Nb}_{1/2})\mathrm{O}_3$–$y\mathrm{PbTiO}_3$–$z\mathrm{PbZrO}_3$ ceramics with x is more than 0·7 showed no peak and smaller value as compared with structural transformation boundary composition. A high radial coupling coefficient over 0·35 was obtained in the region of $x = 0{\cdot}1$ to 0·4 and $z = 0{\cdot}12$ to 0·5 (mole fraction). The highest radial coupling coefficients of each series in Fig. 4 are for the compositions (mole fractions) $z = 0{\cdot}42$ for $x = 0{\cdot}1$, $z = 0{\cdot}34$ for $x = 0{\cdot}2$, $z = 0{\cdot}22$–$0{\cdot}24$ for $x = 0{\cdot}3$, and $z = 0{\cdot}14$ for $x = 0{\cdot}4$.

The foregoing compositions are in good agreement with those exhibiting maxima in electric permittivity. The high radial coupling coefficient thus was obtained near the structural transformation for each compositional series up to $x = 0{\cdot}4$.

The mechanical quality factor (Q_M) and frequency constant (N_p) for the ternary system $x\mathrm{Pb}(\mathrm{Yb}_{1/2}\mathrm{Nb}_{1/2})\mathrm{O}_3$–$y\mathrm{PbTiO}_3$–$z\mathrm{PbZrO}_3$ change with the composition from 24 to 317 and from 1841 to 2774 (Hz·m), respectively.

Q_M and N_p values are low for the composition at which the high radial coupling coefficient and high relative electric permittivity were obtained as shown in Figs 5 and 6, respectively.

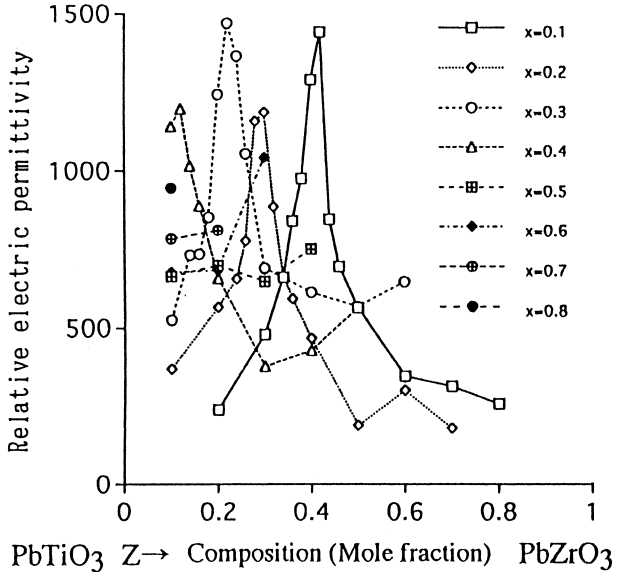

Fig. 3. Relative electric permittivity, $\varepsilon_{33}^T/\varepsilon_0$ for the system $x\mathrm{Pb}(\mathrm{Yb}_{1/2}\mathrm{Nb}_{1/2})\mathrm{O}_3$–$(1-x-z)$ PbTiO_3–$z\mathrm{PbZrO}_3$ with $\mathrm{Pb}(\mathrm{Yb}_{1/2}\mathrm{Nb}_{1/2})\mathrm{O}_3$ as a parameter.

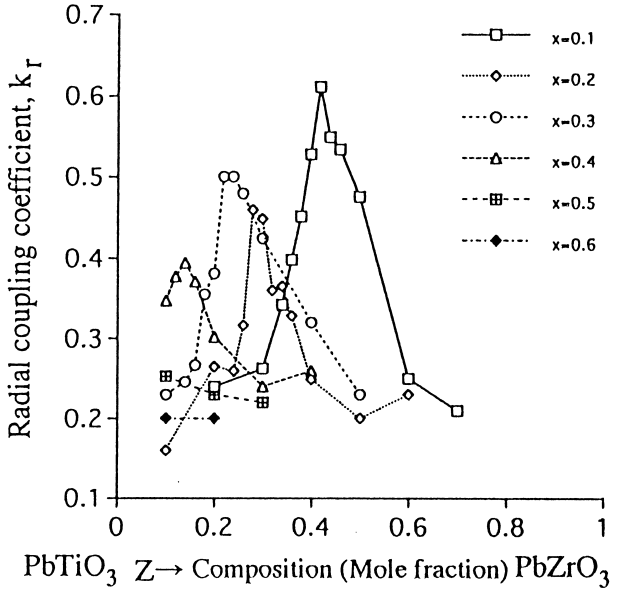

Fig. 4. Radial coupling coefficient for the system $x\mathrm{Pb}(\mathrm{Yb}_{1/2}\mathrm{Nb}_{1/2})\mathrm{O}_3$–$(1-x-z)$ PbTiO_3–$z\mathrm{PbZrO}_3$ with $\mathrm{Pb}(\mathrm{Yb}_{1/2}\mathrm{Nb}_{1/2})\mathrm{O}_3$ as a parameter.

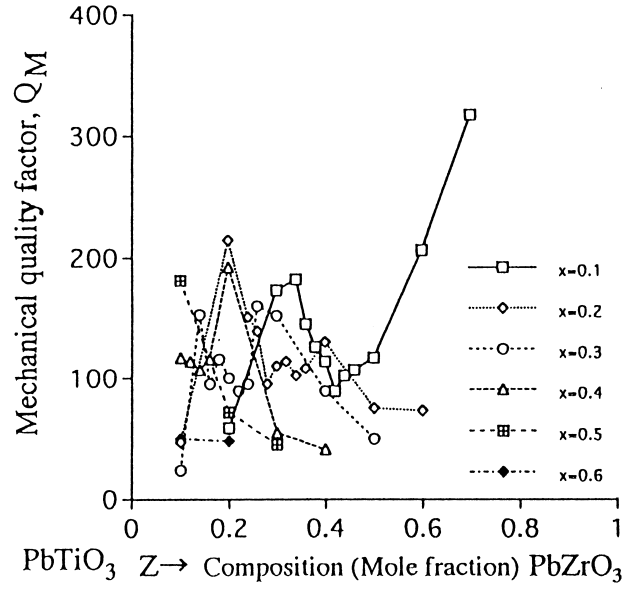

Fig. 5. Mechanical quality factor, Q_M for the system $x\mathrm{Pb}(\mathrm{Yb}_{1/2}\mathrm{Nb}_{1/2})\mathrm{O}_3$–$(1-x-z)$ PbTiO_3–$z\mathrm{PbZrO}_3$ with $\mathrm{Pb}(\mathrm{Yb}_{1/2}\mathrm{Nb}_{1/2})\mathrm{O}_3$ as a parameter.

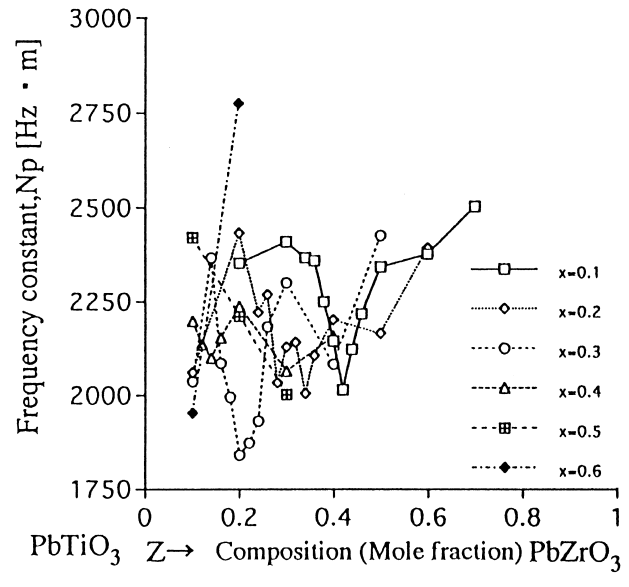

Fig. 6. Frequency constant, Np for the system $x\mathrm{Pb}(\mathrm{Yb}_{1/2}\mathrm{Nb}_{1/2})\mathrm{O}_3$–$(1-x-z)$ PbTiO_3–$z\mathrm{PbZrO}_3$ with $\mathrm{Pb}(\mathrm{Yb}_{1/2}\mathrm{Nb}_{1/2})\mathrm{O}_3$ as a parameter.

The composition $Pb(Yb_{1/2}Nb_{1/2})_{0\cdot1}Ti_{0\cdot48}Zr_{0\cdot42}O_3$ showed the high relative electric permittivity ($\varepsilon_{33}^T/\varepsilon_0 = 1440$), highest radial coupling coefficient ($k_r = 0\cdot61$), lower $Q_M = 89$, lower $N_p = 2010$ (Hz·m) and Curie point $T_c = 395°C$.

4 Conclusions

The present study led to the following conclusions:

1. Sintering of the ternary system $xPb(Yb_{1/2}Nb_{1/2})O_3$–$yPbTiO_3$–$zPbZrO_3$, where $x = 0\cdot1$–$0\cdot8$, $y = 0\cdot1$–$0\cdot7$, $z = 0\cdot1$–$0\cdot8$ and $x + y + z = 1$, is much easier than sintering each end composition, and well sintered, high density ceramics were easily obtained for compositions near the structural transformations.
2. Phase relation of the ternary system $xPb(Yb_{1/2}Nb_{1/2})O_3$–$yPbTiO_3$–$zPbZrO_3$ is composed of monoclinic, tetragonal and rhombohedral crystal phases. A structural transformation from tetragonal phase to rhombohedral or monoclinic phase is found in the vicinity of $y = 0\cdot48$–$0\cdot42$ mole fraction of $PbTiO_3$ for $x = 0\cdot1$, $0\cdot2$, $0\cdot3$ and $0\cdot4$ mole fraction of $Pb(Yb_{1/2}Nb_{1/2})O_3$.
3. High relative electric permittivity, high radial coupling coefficient, low mechanical quality factor and low frequency constant were obtained at compositions near the structural transformation in the piezoelectric ceramics with new ternary composition. The composition $Pb(Yb_{1/2}Nb_{1/2})_{0\cdot1}Ti_{0\cdot48}Zr_{0\cdot42}O_3$ showed the highest $\varepsilon_{33}^T/\varepsilon_0 = 1440$, and $k_r = 0\cdot61$ and the lowest $Q_M = 89$, lowest $N_p = 2010$ (Hz·m) and a Curie point $T_c = 395°C$.

References

1. Jaffe, B., Roth, R. S. and Marzullo, S., Piezoelectric properties of lead zirconate–lead titanate solid-solution ceramics. *J. Appl. Phys.*, 1954, **25**, 809–810.
2. Jaffe, B., Roth, R. S. and Marzullo, S., Properties of piezoelectric ceramics in the solid-solution series lead titanate lead zirconate–lead oxide: tin oxide and lead titanate–lead hafnate. *J. Res. Natl. Bur. Standars.*, 1955, **55**, 239–254.
3. Smolenskii, G. A. and Agranovkaya, A. I., Dielectric polarization of a number of complex compounds. *Soviet Phys. Solid State.*, 1960, **1**, 1429–1437.
4. Ouchi, H., Nagano, K. and Hayakawa, S., Piezoelectric properties of $Pb(Mg_{1/3}Nb_{2/3})O_3$–$PbTiO_3$–$PbZrO_3$ solid solution ceramics. *J. Am. Ceram. Soc.*, 1965, **48**, 630–635.
5. Ohuchi, H. and Nishida, M., Phase relation and electric properties of $Pb(Mg_{1/3}Ta_{2/3})O_3$–$PbTiO_3$–$PbZrO_3$ Ceramics. *J. Japan Soc. Powder and Metallurgy*, 1993, **40**, 687–692.
6. Yamamoto, T. and Ohashi, S., Dielectric and piezoelectric properties of $Pb(Yb_{1/2}Nb_{1/2})O_3$–$PbTiO_3$ solid solution system. *Jpn. J. Appl. Phys.*, 1995, **34**(1/9B), 5349–5353.
7. Jaffe, H. *et al.*, IRE standards on piezoelectric crystals: measurement of piezoelectric ceramics. Proc. IRE., Vol. 49, 1961, pp. 1161–1169.
8. Kulcsar, F., Electromechanical properties of lead titanate zirconate ceramics modified with certain three- or five-valent additions. *J. Am. Ceram. Soc.*, 1959, **42**, 343–349.